XLIII CILAMCE
21–25, November, 2022
FOZ DO IGUAÇU – PR – BRAZIL

Application of the G/XFEM, quasi-3D theory, and the nonlocal elasticity in the vibration analysis of thick functionally graded nano-plates

Oscar A. G de Suarez[1], Rodrigo Rossi[1]

[1]*Departamento de Engenharia Mecânica da Universidade Federal do Rio Grande do Sul*
Sarmento Leite 425, 90050-070, Porto Alegre/RS, Brasil
oagsuarez@ufrgs.br, rrossi@ufrgs.br

Abstract. In this study, the problem of free vibrations in functionally graded moderately thick nanoplates is addressed. The numerical models are obtained employing the quasi-3D plate theory and the approximation spaces are obtained according to the G/XFEM with PU's with regularity $C^k, k = 1,2$. The choice to use the cited approximation spaces is related to their regularity, which is extremely relevant in non-local dynamic elastic problems. In this sense, the use of approximation spaces obtained with C^0 FEM-Lagrange produces significant differences in the nanoscale result which does not occur in classical or local elasticity. In the case studies, the following effects on the first resonance frequency are analyzed: increase in the nanoplate size, distribution of the biphasic material, and increment of the nanoscale parameter. As a complementary result, the effect of the regularity of the approximation spaces in the verification of the stiffness softening phenomenon is analyzed. The normalized frequencies resulting from those obtained with high order FEM-Lagrange, a semi-analytic solution, and the Hermitian elements (H-FEM) $C^k, k = 1,2$.

Keywords: G/XFEM, quasi 3D nano-plates, non-local elasticity.

1 Introduction

The study of micro and nanostructures and their applications in science and engineering has been of improved in importance over the last two decades due to the super properties observed such as the increase in stiffness, the significant increase in thermal, and electrical conductivity, and the high stiffness/mass ratio. Recent studies in this area were carried out by Arash et al. [1], in the simulation of a gas sensor using the problem of wave propagation in graphene sheets. In Kahrobaiy et al. [2], the authors simulate the resonance frequency and sensitivity of a microcantilever in atomic force microscopes using non-classical continuum mechanics theory.

Recently studies involving Functionally Graded Materials (FGM), see Bever and Duwez [3], address issues of bending, free vibrations, and lateral stability on thin and moderately thick nanoplates modeled with different kinematic theories and using non-local elasticity (see Eringen [4]) were performed by Aghababaei and Reddy [5], Daneshmehr et al. [6], Sobhy M. [7], Nami and Janghorban [8], among others.

In this work, the performance of numerical models obtained with the quasi-3D kinematic theory (see, Neves et al. [9]) and the high regularity approximation spaces obtained using G/XFEM (see, Garcia and Rossi, [10]) are analyzed in the approach to the free vibration problems in moderately thick functionally graded nanoplates. The material properties, in each representative volume (RV), are obtained by the Mori-Tanaka homogenization method, the mixing rule, and a power-law as in Neves et al. [9].

2 Free vibration in quasi 3D functionally graded nanoplates

In this section, the problem of free vibrations of thick and moderately thick nanoplates, Figure 1, modeled with the quasi-3D theory is addressed as in Neves et al. [9]. The functions that describe the displacement fields are defined in the equations Eq. (1)-(3).

$$u\left(x,y,z,t\right) = u_0\left(x,y,t\right) + z\theta_x\left(x,y,t\right) + z^3\gamma_x\left(x,y,t\right) \tag{1}$$

$$v\left(x,y,z,t\right) = v_0\left(x,y,t\right) + z\theta_y\left(x,y,t\right) + z^3\gamma_y\left(x,y,t\right) \tag{2}$$

$$w\left(x,y,z,t\right) = w_0\left(x,y,t\right) + zw_1\left(x,y,t\right) + z^2w_2\left(x,y,t\right) \tag{3}$$

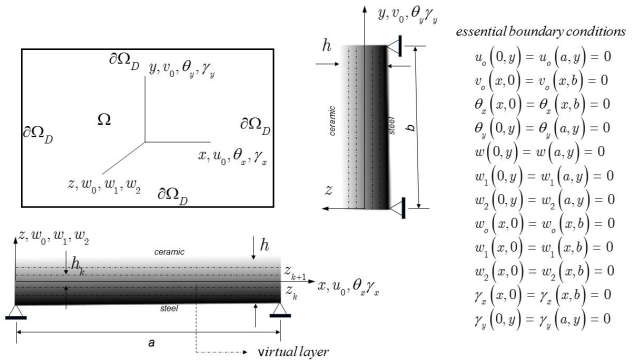

Figure 1: Simply supported functionally graded nanoplate.

Discrete formulation for the quasi 3D functionally graded nanoplate

The discrete formulation is obtained by the Galerkin Finite Element Method where the fields that describe the components of displacements in an element "e" are defined by Eq.(4)-(10), using the shape functions shown in Garcia and Rossi [10].

$$\boldsymbol{u}_e \cong \boldsymbol{u}_{eh} = \boldsymbol{N}_e^{(0)}\boldsymbol{U}_e,\ \boldsymbol{N}_e^{(0)} = \begin{bmatrix} \cdots & \psi_i^j & 0 & 0 & 0 & 0 & 0 & 0 & 0 & \cdots \\ \cdots & 0 & \psi_i^j & 0 & 0 & 0 & 0 & 0 & 0 & \cdots \end{bmatrix} \tag{4}$$

$$\boldsymbol{\psi}_e \simeq \boldsymbol{\psi}_{eh} = \boldsymbol{N}_e^{(1)}\boldsymbol{U}_e,\ \boldsymbol{N}_e^{(1)} = \begin{bmatrix} \cdots & 0 & 0 & 0 & \psi_i^j & 0 & 0 & 0 & 0 & \cdots \\ \cdots & 0 & 0 & 0 & 0 & \psi_i^j & 0 & 0 & 0 & \cdots \end{bmatrix} \tag{5}$$

$$\boldsymbol{\gamma}_e \simeq \boldsymbol{\gamma}_{eh} = \boldsymbol{N}_e^{(3)}\boldsymbol{U}_e,\ \boldsymbol{N}_e^{(3)} = \begin{bmatrix} \cdots & 0 & 0 & 0 & 0 & 0 & 0 & 0 & \psi_i^j & 0 & \cdots \\ \cdots & 0 & 0 & 0 & 0 & 0 & 0 & 0 & 0 & \psi_i^j & \cdots \end{bmatrix} \tag{6}$$

$$w_{eo} \simeq w_{oeh} = \boldsymbol{N}_{es}^{(0)}\boldsymbol{U}_e,\ \boldsymbol{N}_{es}^{(0)} = \begin{bmatrix} \cdots & 0 & 0 & \psi_i^j & 0 & 0 & 0 & 0 & 0 & 0 & \cdots \end{bmatrix} \tag{7}$$

$$w_{1e} \simeq w_{1eh} = \boldsymbol{N}_{es}^{(1)}\boldsymbol{U}_e,\ \boldsymbol{N}_{es}^{(1)} = \begin{bmatrix} \cdots & 0 & 0 & 0 & 0 & 0 & \psi_i^j & 0 & 0 & 0 & \cdots \end{bmatrix} \tag{8}$$

$$w_{2e} \simeq w_{2eh} = \boldsymbol{N}_{es}^{(2)}\boldsymbol{U}_e,\ \boldsymbol{N}_s^{(2)} = \begin{bmatrix} \cdots & 0 & 0 & 0 & 0 & 0 & 0 & \psi_i^j & 0 & 0 & \cdots \end{bmatrix} \tag{9}$$

$$\boldsymbol{U}_e^T = \left\{\cdots \quad u_i^j \quad v_i^j \quad w_i^j \quad \theta_{xi}^j \quad \theta_{yi}^j \quad w_{1i}^j \quad w_{2i}^j \quad \gamma_{ix}^j \quad \gamma_{iy}^j \quad \cdots\right\},\ i = 1,...,N_e \ \ j = 0,...,p\,. \tag{10}$$

In Eq. (10) N_e is the number of enriched nodes of the element and p is the polynomial order of the enrichment functions. The discrete formulation of normal strains for points inside an element is shown in a generic way by Eq. (12).

$$\varepsilon_e^{(i)} = \left\{\frac{\partial U_e}{\partial x} \quad \frac{\partial V_e}{\partial y} \quad \frac{\partial U_e}{\partial y} + \frac{\partial V_e}{\partial x}\right\}^T = \boldsymbol{B}_e^{(i)}\boldsymbol{U}_e,\ i = 0,1,3\,. \tag{11}$$

In this equation, the generic field functions U_e, V_e represent the components of vector functions $\boldsymbol{u}^T(u_0,\ v_0)$, $\boldsymbol{\psi}^T(\theta_x, \theta_y)$, and $\boldsymbol{\gamma}^T(\gamma_x, \gamma_y)$ respectively to the index $i = 0,1,3$. The deformation matrix $\boldsymbol{B}_e^{(i)}$ is shown in matrix notation in Eq (12), being the operators $\boldsymbol{H}$, $\boldsymbol{J}$, and $\boldsymbol{\partial}_\varsigma$ defined as in Garcia and Rossi [10].

$$\boldsymbol{B}_e^{(i)} = \boldsymbol{H}\boldsymbol{J}\partial_\varsigma \boldsymbol{N}_e^{(i)},\ i = 0,1,3\,. \tag{12}$$

The gradients of the scalar and vector functions as well the components of shear strain and normal strain in the thickness direction are described in Eq. (12)-(17). In Eq. (12), $\partial_s = \{\partial(\,.\,)/\partial\xi \quad \partial(\,.\,)/\partial\eta\}^T$ and J is the Jacobian matrix. In Eq. (14), $\nabla\boldsymbol{L}^{(0)} = \nabla\boldsymbol{u}$, $\nabla\boldsymbol{L}^{(1)} = \nabla\boldsymbol{\psi}$, and $\nabla\boldsymbol{L}^{(3)} = \nabla\boldsymbol{\gamma}$.

$$\nabla\boldsymbol{w}_e^{(i)} = \boldsymbol{G}_{se}^{(i)}U_e,\ \ \boldsymbol{G}_{se}^{(i)} = J^{-1}\partial_s\boldsymbol{N}_{se}^{(i)},\ i = 0,1,2 \tag{13}$$

$$\nabla\boldsymbol{L}^{(i)} \cong \boldsymbol{G}_e^{(i)}\boldsymbol{U}_e,\ \boldsymbol{G}_e^{(i)} = \boldsymbol{J}\partial_\varsigma\boldsymbol{N}^{(i)},\ i = 0,1,3 \tag{14}$$

$$\boldsymbol{\varepsilon}_{se}^{(0)} = \left\{\gamma_{xz} \quad \gamma_{yz} \quad w_1\right\}_e^T \cong \left[B_{se}^{(0)} \quad \boldsymbol{N}_{se}^{(1)}\right]^T\boldsymbol{U}_e,\ \boldsymbol{B}_{se}^{(0)} = \left[B_{se}^{(0)} \quad \boldsymbol{N}_{se}^{(1)}\right]^T \tag{15}$$

$$\boldsymbol{\varepsilon}_{se}^{(1)} = \left\{\frac{\partial w_1}{\partial x} \quad \frac{\partial w_1}{\partial y} \quad 2w_2\right\}_e^T \cong \begin{bmatrix}\boldsymbol{G}_e^{(1)} \\ 2\boldsymbol{N}_{se}^{(2)}\end{bmatrix}\boldsymbol{U}_e = \boldsymbol{B}_{se}^{(1)}\boldsymbol{U}_2,\ \boldsymbol{B}_{se}^{(1)} = \begin{bmatrix}\boldsymbol{G}_e^{(1)} \\ 2\boldsymbol{N}_{se}^{(2)}\end{bmatrix},\ \boldsymbol{G}_e^{(1)} = J^{-1}\partial_s\boldsymbol{N}_{se}^{(1)} \tag{16}$$

$$\boldsymbol{\varepsilon}_{se}^{(2)} = \left\{\frac{\partial w_2}{\partial x} + 3\gamma_x \quad \frac{\partial w_2}{\partial y} + 3\gamma_y \quad 0\right\}^T \cong \boldsymbol{B}_{se}^{(2)}\boldsymbol{U}_e, \boldsymbol{B}_{se}^{(2)} = \left(\begin{bmatrix}\boldsymbol{G}_e^{(2)} \\ 0\end{bmatrix} + \begin{bmatrix}3\boldsymbol{N}_e^{(3)} \\ 0\end{bmatrix}\right). \tag{17}$$

The constitutive equation is described by Eq. (18), for the *k-th* layer, using the vectors of internal forces "S_k" according to Neves et al. [9]. On the other hand, the Galerkin integral shown in Eq. (23) is obtained from Eqs. (4)-(22). In this approach the mass inertia moments $I_{ik}, i = 0,1,2,3,4,6$ are shown in Eq. (22). On the other hand, the essential boundary conditions are weakly imposed by the external penalty method where the penalty multiplier λ_i $i = 0,1,2,3,4,6$ are shown in Eq. (22), being α the penalty coefficient.

$$\underbrace{\begin{Bmatrix} \boldsymbol{N}_k \\ \boldsymbol{M}_k \\ \boldsymbol{R}_k \\ \boldsymbol{Q}_k \\ \boldsymbol{M}_{sk} \\ \boldsymbol{R}_{sk} \end{Bmatrix}}_{\boldsymbol{s}_k} = \underbrace{\begin{bmatrix} \boldsymbol{A}_k^{(1)} & \boldsymbol{B}_k^{(1)} & \boldsymbol{E}_k^{(1)} & \boldsymbol{A}_k^{(2)} & \boldsymbol{B}_k^{(2)} & \mathbf{0} \\ \boldsymbol{B}_k^{(1)} & \boldsymbol{D}_k^{(1)} & \boldsymbol{F}_k^{(1)} & \boldsymbol{B}_k^{(2)} & \boldsymbol{D}_k^{(2)} & \mathbf{0} \\ \boldsymbol{E}_k^{(1)} & \boldsymbol{F}_k^{(1)} & \boldsymbol{G}_k^{(1)} & \boldsymbol{E}_k^{(2)} & \boldsymbol{F}_k^{(2)} & \mathbf{0} \\ \boldsymbol{A}_k^{(3)} & \boldsymbol{B}_k^{(3)} & \boldsymbol{E}_k^{(3)} & \boldsymbol{A}_k^{(4)} & \boldsymbol{B}_k^{(4)} & \boldsymbol{D}_k^{(4)} \\ \boldsymbol{B}_k^{(3)} & \boldsymbol{D}_k^{(3)} & \boldsymbol{F}_k^{(3)} & \boldsymbol{B}_k^{(4)} & \boldsymbol{D}_k^{(4)} & \boldsymbol{E}_k^{(4)} \\ \mathbf{0} & \mathbf{0} & \mathbf{0} & \boldsymbol{B}_k^{(5)} & \boldsymbol{D}_k^{(5)} & \boldsymbol{E}_k^{(5)} \end{bmatrix}}_{\boldsymbol{C}_k} \underbrace{\begin{Bmatrix} \varepsilon_e^{(0)} \\ \varepsilon_e^{(1)} \\ \varepsilon_e^{(3)} \\ \varepsilon_{se}^{(0)} \\ \varepsilon_{se}^{(1)} \\ \varepsilon_{se}^{(2)} \end{Bmatrix}}_{\varepsilon} \tag{18}$$

In Eq. (18), the constitutive submatrices, $A_k^{(i)}, \boldsymbol{B}_k^{(j)}, \boldsymbol{D}_k^{(l)}, \boldsymbol{E}_k^{(m)}, \boldsymbol{F}_k^{(n)}$, and $\boldsymbol{G}_k^{(p)}$, $i = 1,..,4, j = 1,...,5, l = 1,...,5, m = 1,...,5, n = 1,...,3, p = 1$, that make up the constitutive matrix $\mathbf{C}_k$, are obtained in a generic way by Eq. (19)-(21), from the constitutive matrices $\boldsymbol{A}_k, \boldsymbol{B}_k, \boldsymbol{D}_k, \boldsymbol{E}_k, \boldsymbol{F}_k$, and $\boldsymbol{G}_k$ described in Neves et al. [9].

$$\boldsymbol{M}_k^{(1)} = \begin{bmatrix} M_{11} & M_{12} & 0 \\ M_{12} & M_{22} & 0 \\ 0 & 0 & M_{33} \end{bmatrix}, \boldsymbol{M}_k^{(2)} = \begin{bmatrix} 0 & 0 & M_{16} \\ 0 & 0 & M_{26} \\ 0 & 0 & 0 \end{bmatrix}, \boldsymbol{M}_k^{(3)} = \begin{bmatrix} 0 & 0 & 0 \\ 0 & 0 & 0 \\ M_{16} & M_{26} & 0 \end{bmatrix} \tag{19}$$

$$\boldsymbol{M}_k^{(4)} = \begin{bmatrix} M_{44} & 0 & 0 \\ 0 & M_{55} & 0 \\ 0 & 0 & M_{66} \end{bmatrix}, \boldsymbol{M}_k^{(5)} = \begin{bmatrix} M_{44} & 0 & 0 \\ 0 & M_{55} & 0 \\ 0 & 0 & 0 \end{bmatrix} \tag{20}$$

$$\boldsymbol{M}_k^{(i)} \equiv \boldsymbol{A}_k^{(i)}, \boldsymbol{B}_k^{(i)}, \boldsymbol{D}_k^{(i)}, \boldsymbol{E}_k^{(i)}, \boldsymbol{F}_k^{(i)}, \boldsymbol{G}_k^{(i)}, \ i = 1,...,5 \tag{21}$$

$$I_{ik} = \int_{z_k}^{z_{k+1}} \rho_k z^i dz, \ \lambda_i = \int_{-h/2}^{h/2} z^i \alpha \delta_n dz, \ , \ \delta_n = \begin{cases} 1, & \text{presc ndof} \\ 0, & \text{n/presc ndof} \end{cases} \ n = 1,...,9 \tag{22}$$

$$\left\{ \underbrace{\sum_{e=1}^{N_e} \sum_{k=1}^{N_l} \left(\boldsymbol{b}_e^{(0)T} + \boldsymbol{b}_e^{(1)T} + \boldsymbol{b}_e^{(3)T} + \boldsymbol{b}_{se}^{(0)T} + \boldsymbol{b}_{se}^{(1)T} + \boldsymbol{b}_{se}^{(2)T} \right) \boldsymbol{C}_k \boldsymbol{B}_e d\Omega}_{\boldsymbol{K}} + \underbrace{\sum_{e=1}^{Ne} \left(\int_{\Omega_e} \boldsymbol{N}_e^T \boldsymbol{\Lambda}_n \boldsymbol{N}_e d\Omega \right.}_{\boldsymbol{K}_\lambda} \right.$$

$$\left. \underbrace{\int_{\Omega_e} \boldsymbol{N}_{se}^T \boldsymbol{\Lambda}_s \boldsymbol{N}_s d\Omega \right)}_{\boldsymbol{K}_\lambda} - \omega^2 \left[\underbrace{\sum_{e=1}^{N_e} \sum_{k=1}^{N_l} \left(\int_{\Omega_e} \boldsymbol{N}_e^T \boldsymbol{I}_{nk} \boldsymbol{N}_e d\Omega + \int_{\Omega_e} \boldsymbol{N}_{se}^T \boldsymbol{I}_{sk} \boldsymbol{N}_{se} d\Omega \right)}_{\boldsymbol{M}_L} \right.$$

$$\left. \left. + \mu \underbrace{\sum_{e=1}^{N_e} \sum_{k=1}^{N_l} \left(\int_{\Omega_e} \boldsymbol{G}_e^T \boldsymbol{I}_{nk} \boldsymbol{G}_e d\Omega + \int_{\Omega_e} \boldsymbol{G}_{se}^T \boldsymbol{I}_{sk} \boldsymbol{G}_{se} \right)}_{\boldsymbol{M}_{NL}} \right] \right\} \boldsymbol{U} = 0, \quad \boldsymbol{U} \in R^N \tag{23}$$

In Eq. (23), $\boldsymbol{U}$ is the global vector of displacement parameters, N is the number of degrees of freedom of the numerical mode, ω is the natural frequency and μ is the nanoscale coefficient. In this equation, $\boldsymbol{K}$ and $\boldsymbol{K}_\lambda$ are the stiffness and penalty matrices and $\boldsymbol{M}_L$ and $\boldsymbol{M}_{NL}$ are local and non-local mass matrices, respectively.

$$\boldsymbol{b}_e^{(i)} = \begin{bmatrix} \mathbf{0} & \cdots & \boldsymbol{B}_{ej}^{(i)} & \cdots & \mathbf{0} & \mathbf{0} \end{bmatrix}_{(1\times 6)},\ j = i+1,\ i < 3,\ i = 3, j = i,\ i = 0,1,3. \tag{24}$$

$$\boldsymbol{B}_e = \begin{bmatrix} \boldsymbol{B}_e^{(0)} & \boldsymbol{B}_e^{(1)} & \boldsymbol{B}_e^{(3)} & \boldsymbol{B}_{se}^{(0)} & \boldsymbol{B}_{se}^{(1)} & \boldsymbol{B}_{se}^{(2)} \end{bmatrix}^T \tag{25}$$

$$\boldsymbol{b}_{se}^{(i)} = \begin{bmatrix} \mathbf{0} & \cdots & \boldsymbol{B}_{sej}^{(i)} & \cdots & \mathbf{0} & \mathbf{0} \end{bmatrix}_{(1\times 6)},\ j = i+4,\ i = 0,1,2 \tag{26}$$

$$\boldsymbol{N}_e = \begin{bmatrix} \boldsymbol{N}_e^{(0)} & \boldsymbol{N}_e^{(1)} & \boldsymbol{N}_e^{(3)} \end{bmatrix}^T,\ \boldsymbol{N}_{se} = \begin{bmatrix} \boldsymbol{N}_{se}^{(0)T} & \boldsymbol{N}_{se}^{(1)T} & \boldsymbol{N}_{se}^{(2)T} \end{bmatrix}^T, \tag{27}$$

$$\boldsymbol{G}_e = \begin{bmatrix} \boldsymbol{G}_e^{(0)} & \boldsymbol{G}_e^{(1)} & \boldsymbol{G}_e^{(3)} \end{bmatrix}^T,\ \boldsymbol{G}_{se} = \begin{bmatrix} \boldsymbol{G}_e^{(0)} & \boldsymbol{G}_e^{(1)} & \boldsymbol{G}_e^{(2)} \end{bmatrix}^T \tag{28}$$

$$\boldsymbol{\Lambda}_n = \begin{bmatrix} \lambda_0 & \lambda_1 & \lambda_3 \\ \lambda_1 & \lambda_2 & \lambda_4 \\ \lambda_3 & \lambda_4 & \lambda_6 \end{bmatrix},\ \boldsymbol{\Lambda}_s = \begin{bmatrix} \lambda_0 & \lambda_1 & \lambda_2 \\ \lambda_1 & \lambda_2 & \lambda_3 \\ \lambda_2 & \lambda_3 & \lambda_4 \end{bmatrix},\ \boldsymbol{I}_{nk} = \begin{bmatrix} I_{0k} & I_{1k} & I_{3k} \\ I_{1k} & I_{2k} & I_{4k} \\ I_{3k} & I_{4k} & I_{6k} \end{bmatrix},\ \boldsymbol{I}_{sk} = \begin{bmatrix} I_{0k} & I_{1k} & I_{2k} \\ I_{1k} & I_{2k} & I_{3k} \\ I_{2k} & I_{3k} & I_{4k} \end{bmatrix} \tag{29}$$

3 Numerical Results

Numerical results are referred to the plate shown in Figure *1*, with aspect ratios $a/b = 1$ and $a/h = 20$. Constituent materials and their physical properties are shown in Table 1.

Table 1: Physical properties of materials.

Materials	Properties		
	$E\left(GPa\right)$	$\rho\left(Kg\,/\,m^3\right)$	ν
$S_{i3}N_4$	348.86	2370	0.32
SUS-300	201.4	8166	0.32

Numerical results for all examples presented are obtained by the strategies indicated in Table 2.

Table 2: Numerical strategies obtained by "*p*" homogeneous version.

model	Element Type	Num. Elements	p	NDOF
A	Q4	10×10	$m = 20, n = 20$	3600
B	Q4	5×5	3	3240
C	Q4	5×5	3	3240
D	Q16	7×7	3	3600
E	Q4	5×5	5	3840

In Table 2:

A. Semi-analytic solution obtained by bi-harmonic Navier modes and Bubnov-Galerkin Method.
B. Approximation space with C^2 regularity obtained by the "*p*" homogeneous version conforming G/XFEM.
C. Approximation space with C^4 regularity obtained by the "*p*" homogeneous version conforming G/XFEM.
D. Approximation space obtained by Q16 Lagrange Finite Elements with C^0 regularity.
E. Approximation space obtained by Hermite Finite Elements with C^2 regularity.

Influence of dimensions and the graduation of biphasic material on resonant frequency

In this study, the convergence of the first resonant frequency is analyzed using the ratio $F_r = \omega_{NL}/\omega_L$ (ω_{NL}, ω_L, non-local frequency and local frequency respectively) with the increment of the nanoplate dimensions and the influence of the functionally graded of the biphasic material on the first normalized resonant frequency $\omega = \omega_1 h\sqrt{\rho_c/E_c}$ (ρ_c and E_c are the volumetric mass and the Young modulus of the ceramic material) for the B strategy approximation spaces. Figure 2(a) shows the convergence of the F_r curves obtained with non-local elasticity with increasing plate dimensions as predicted by Eringen C. [4]. On the other hand, Figure 2(b) shows a decay of the stiffness produced by the increasing of the power-law exponent "n" (see, Neves et al. [9]) and by the stiffness-softening phenomenon produced by the increasing of μ.

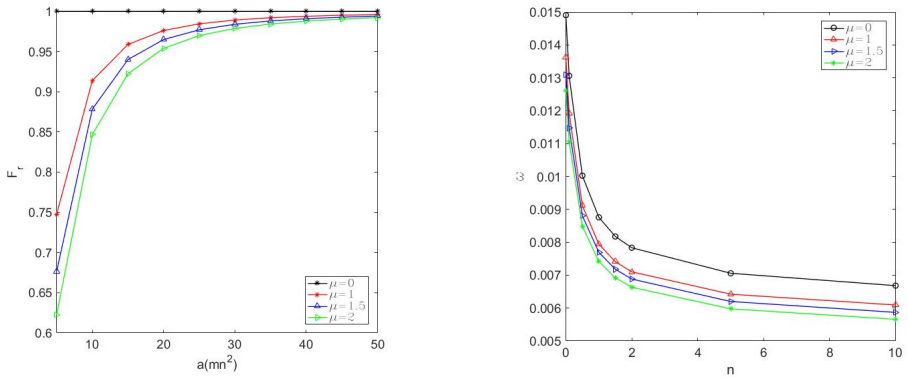

(a) (b)

Figure 2: a) normalized resonant frequency variation *vs.* coplanar dimensions, b) normalized resonant frequency *vs.* power "n".

3.1 Simulation of the Stiffness-Softening phenomenon

The stiffness softening phenomenon is verified by a relaxation of stiffness, denoted by the frequency decay, when the effects produced by the nanoscale are considered.

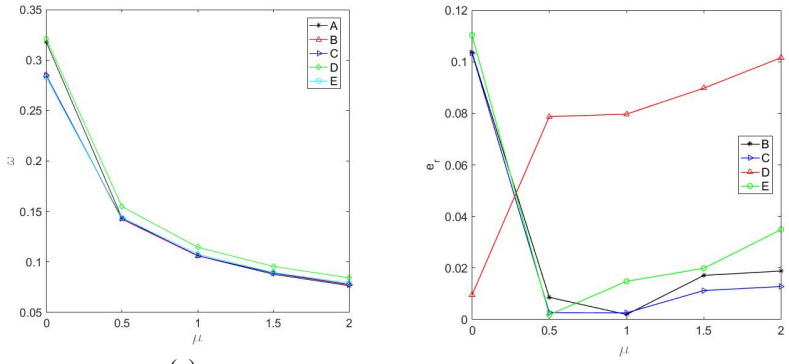

(a) (b)

Figura 3: a) normalized frequency *vs.* nanoscale factor; b) relative error *vs.* nanoscale factor.

In this study, the effect of the smoothness of the approximation spaces (strategies B, C, D, E) is verified by analyzing the decay of the ninetieth normalized frequency $\omega = \omega_{90} h\sqrt{\rho_c/E_c}$ with the increment of the nanoscale factor μ. The effect of smoothness is analyzed by the relative error $e_r = |\omega_h - \omega_a|/|\omega_a|$, where ω_a is obtained by strategy A and ω_h by the above-cited strategies. The stiffness-softening results are shown for strategies A through E in Figura 3(a) where a more accentuated decay is observed in the $(\omega \times \mu)$ curves of strategies A, B, D,

and E than that obtained with strategy C. On the other hand, in Figura 3(b), shows a superior convergence of strategies B, C, and E with respect to strategy D (FEM C^0). The superiority of the results is due to the incorporation of the gradients of the shape functions in the non-local mass matrix.

4 Conclusions

The mechanical behavior of functionally graded moderately thick nanoplates was numerically investigated by using the almost 3D kinematic model with an extensible normal and by approximation spaces obtained with the homogeneous p version of G/XFEM with regularity $C^k, k = 2,4,$. The convergence results confirm the non-local theory of elasticity of Eringen (1983). The stiffness-softening phenomenon was observed and represented by the variation of the nanoscale coefficient. Finally, the effect of regularity is relevant to the results at the nanoscale. In this context, the results obtained with G/XFEM were significantly superior to those obtained by other approximation spaces, such as the FEM-Lagrange, and slightly superior to those obtained with HFEM.

Acknowledgements. The authors of this work would like to thank CAPES for financial support through the postdoctoral scholarship and the infrastructure provided by UFRGS. Also, to the CNPq and FAPERGS for financial research support. Grant numbers: CNPq 309430/2021-6 and FAPERGS: 19/2551-0001954-8-1

References

[1] B. Arash, K. Wang and K. M. Liew, "Wave propagation in graphene sheets with nonlocal elastic theory via finite element formulation," *Computer Method in Applied Mechanics and Engineerig,* vol. 224, pp. 1-9, 2012.

[2] M. H. Kahrobaiyan, M. Asghari, M. Rahaeifard and M. T. Ahmadian, "Investigation of the size-dependent dynamic characteristics of atomic force microscope microcantilevers based on the modified couple stress theory," *International Journal of Engineering Science,* vol. 48, pp. 1985-1994.

[3] M. B. Bever and P. E. Duwez, "Gradients in composite materials," *Material Science and Engineerig,* vol. 10, pp. 1-8, 1972.

[4] A. C. Eringen, "On differential equations of nonlocal elasticity and solutions of screw dislocation and surface waves," *Journal of Applied Physic,* vol. 54, pp. 4703-4710, 1983.

[5] R. Aghababaei and J. N. Reddy, "Nonlocal third-order shear deformation plate theory with application to bending and vibration of plates," *Journal of Sound and Vibration,* vol. 326, pp. 277-289, 2009.

[6] A. Daneshmehr, A. Rajabpoor and M. pourdavood, "Stability of size dependent functionally graded nanoplate based on nonlocal elasticity and higher order plate theories and different boundary conditions," *International Journal of Engineering Science,* vol. 82, pp. 84-100.

[7] M. Sobhy, "A comprehensive study on FGM nanoplates embedded in an elastic medium," *Composite Structures,* vol. 143, pp. 966-980, 2015.

[8] R. M. Nami and M. Janghorban, "Resonance behavior of FG rectangular micro/nano plate based on nonlocal elasticity theory and strain gradient theory with one gradient constant," *Composite Structures,* vol. 111, pp. 349-353, 2014.

[9] A. M. A. Neves, A. M. Ferreira, E. Carrera, M. Cinefra, C. C. Roque, R. N. Jorge and C. M. Soares, "Static, free vibration and buckling analysis of isotropic and sandwich functionally graded plates using a quasi-3D higher-order shear deformation theory and a meshless technique," *Composites: Part B,* vol. 44, pp. 657-674, 2013.

[10] O. A. Garcia and R. Rossi, "A G/XFEM approximation space based on the enrichment of rational polynomials to model free and forced vibration in elastic isotropic Mindlin–Reissner plates," *Journal of the Brazilian Society of Mechanical Sciences and Engineering,* vol. 34, p. 134, 2019.

Authorship statemen. The authors confirm that they are solely responsible for the authorship of this work, and that all material that has been included here as part of this paper is either owned (and authored) by the authors or has the permission of the owners to be included here.